PHYSICAL REVIEW C **87**, 041305(R) (2013)

Shape coexistence in neutron-rich nuclei near $N = 40$

M. P. Carpenter, R. V. F. Janssens, and S. Zhu
Physics Division, Argonne National Laboratory, Argonne, Illinois 60439, USA
(Received 5 April 2013; published 29 April 2013)

Recent data show that both the 2^+ and 4^+ levels in the even neutron-rich Cr and Fe isotopes decrease in excitation energy toward $N = 40$. This observation, along with Coulomb excitation and lifetime data, strongly indicates an increase in collectivity near $N = 40$ in contradiction with expectations based on first principles. A straightforward two-band mixing model is used to investigate the structure of these neutron-rich Cr and Fe nuclei. The approach takes advantage of the extensive data available for ^{60}Fe to provide the parameter values with which to reproduce the experimental observations in the $^{58-64}$Cr and $^{60-68}$Fe isotopic chains. Comparisons between the model and the data suggest marked structural differences for the ground-state configurations of $N = 40$ Cr and Fe.

DOI: 10.1103/PhysRevC.87.041305 PACS number(s): 21.10.Re, 21.60.−n, 27.50.+e

Numerous studies have recently focused on understanding the structure of neutron-rich nuclei in the fp shell between Ca and Ni. Of particular note is the observation of a $N = 32$ subshell closure in ^{52}Ca, ^{54}Ti, and ^{56}Cr [1–3]. Recent measurements have also tracked the excitation energy of the first 2^+ and 4^+ states in the Cr and Fe isotopes up to neutron number $N = 40$ [4] and $N = 42$ [5], respectively. In both isotopic chains, these energies decrease with increasing N, suggesting the onset of collectivity near $N = 40$. In fact, $N = 40$ ^{64}Cr exhibits the lowest 2_1^+ excitation energy in nuclei of the region and appears to be deformed in its ground state. In contrast, its isotone ^{68}Ni exhibits most of the characteristics of a doubly magic nucleus [6]. Lifetime information obtained for the 2^+ states in ^{62,64,66}Fe [7,8] and ^{60,62}Cr [9] as well as proton inelastic scattering data on ^{60,62}Cr [10] support this interpretation. In addition, β-decay measurements have identified low-lying states in odd-A Fe [11] and odd-odd Mn isotopes [12] near $N = 40$ which have been associated with deformed Nilsson configurations based on spin/parity arguments. Shell-model calculations with a neutron valence space limited to the fp shell are unable to reproduce the experimental observations, in contrast to those expanding the space to include both $g_{9/2}$ and $d_{5/2}$ neutrons [13–15].

In addition, a sequence of measurements with the Gammasphere array has identified high-spin states in neutron-rich Cr, Mn, Fe, and Ni isotopes between $N = 32$ and 40 using both fusion-evaporation and deep-inelastic reactions [6,15–21]. A number of rotational bands, including some associated with large deformation, have been found. The configurations of these bands are reported to contain as least one $g_{9/2}$ neutron. In this paper, a connection is proposed between the rotational bands observed in the Cr and Fe nuclei for $N = 32$–36 and the low-spin yrast structures observed in the heavier isotopes. A straightforward two-band mixing model is applied to show that these Cr and Fe isotopes with $N = 34$–42 exhibit properties similar to those observed in other mass regions where coexistence between well-deformed and near-spherical shapes occurs.

Shape coexistence is observed in a number of regions of the nucleonic chart, quite often near the bottom or top of a shell, where deformed structures are found to compete with those associated with the spherical shape preferred at shell closures. For example, in neutron mid-shell ($N \sim 102$) Hg-Pb nuclei, which are at or near the top of the $Z = 82$ proton shell, excitations associated with spherical, prolate, and oblate shapes are found to coexist near the ground state [22]. In a few cases, evidence for all three shapes is observed in a single nucleus [23]. As a general rule, this shape coexistence is most readily seen in systems where the ground state is spherical or weakly deformed. This is due to the fact that the deformed structure, with its large moment of inertia, quickly becomes yrast and dominates the level structure at moderate and high spins. Figure 1 illustrates this point for the even-even Hg isotopes by presenting the spin along the rotational axis, I_x, as a function of the rotational frequency, $\hbar\omega$, and the large "backbending" behavior results from the crossing of the weakly deformed ground-state sequence by a prolate-deformed rotational band.

Figure 2 provides the same plot for all known yrast levels in the even-even Cr and Fe isotopes with $N = 34$–42 [4,5,15,17–19]; clear similarities can be noticed between Figs. 1 and 2 for the Fe isotopes. In the Cr isotopes, the data are more limited but are consistent with the same interpretation, as will be discussed hereafter. The number of known states along the yrast line differs from nucleus to nucleus due to the types of reactions used to populate the levels of interest. For example, ^{60}Fe has been observed to the highest spins seen thus far because its excited states were populated with a heavy-ion-induced fusion-evaporation reaction [19]. In contrast, the sequences in ^{62,64}Fe have only been observed up to $I \sim 10\hbar$ as they were populated through deep-inelastic collisions [15,18]. In fact, for the most neutron-rich isotopes, the highest levels populated are limited to spins of 4 or 6 $\hbar$, since the relevant data come from either reactions with fast secondary beams or β decay. The situation for the Cr isotopes is similar.

For the present purpose, ^{60}Fe is most instructive with its clear backbending behavior (Fig. 2). As discussed in Ref. [19], the yrast states up to the 6^+ level are described well by shell-model calculations with the GXPF1A Hamiltonian which is restricted to orbitals within the fp shell and excludes higher-lying states such as $g_{9/2}$ neutrons. However, the higher-spin states, between $I^\pi = 8^+$ and 20^+, have little

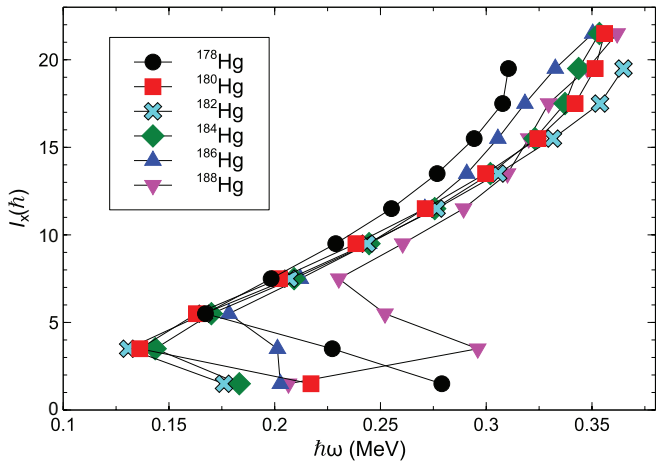

FIG. 1. (Color online) Spin along the rotational axis, I_x, as a function of the rotational frequency, $\hbar\omega$, for the yrast sequences of Hg isotopes. The data are taken from Refs. [24–28].

correspondence with the shell model [19]. In addition, these levels form a smooth sequence reminiscent of the behavior exhibited by the prolate rotational structures in the Hg isotopes (Fig. 1). Consequently, these states have been interpreted as belonging to a rotational band built on a $(g_{9/2})^2$ aligned neutron configuration, and total Routhian surface (TRS) calculations

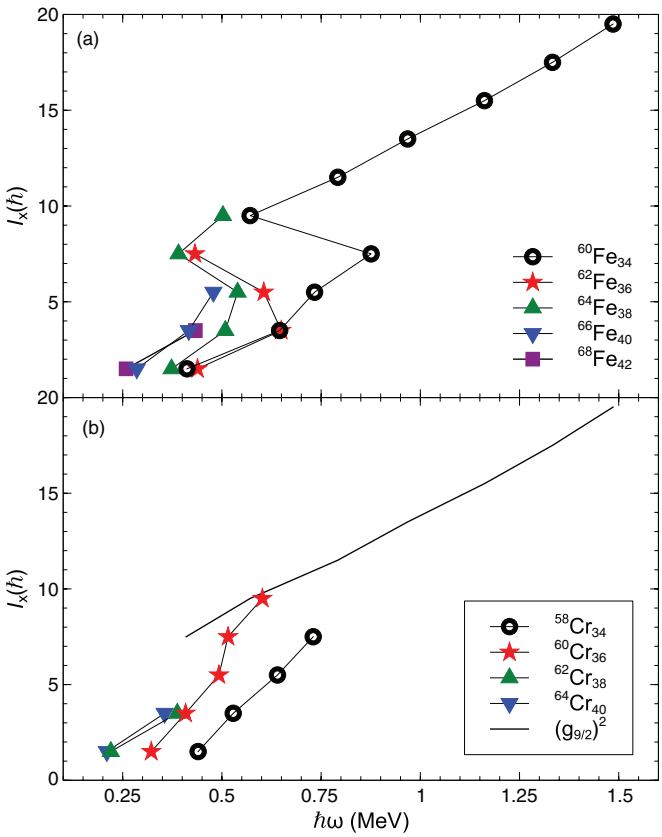

FIG. 2. (Color online) Same as Fig. 1, but for the (a) Fe and (b) Cr isotopes. The $(g_{9/2})^2$ solid line is taken from the yrast band in ^{60}Fe for $I = 8$–$20\ \hbar$ (see text for details). The data are taken from Refs. [4,5,15,17–19].

support this interpretation [19]. In this case, the $(g_{9/2})^2$ configuration is associated with an axial symmetric shape with $\beta_2 \sim 0.2$ deformation [19]. The importance of ^{60}Fe cannot be stressed enough as it provides information on trajectories in the I_x vs ω plane to be expected for excitations associated with both the shell model and the deformed shape.

When comparing the behavior of the yrast sequences in the heavier Fe isotopes to that of ^{60}Fe, an interpretation of the 8^+ state in ^{62}Fe and the 8^+ and 10^+ levels in ^{64}Fe readily presents itself. From Fig. 2 it is clear that these states lie on the trajectory defined by the $(g_{9/2})^2$ band in ^{60}Fe indicating that for $I^\pi \geqslant 8^+$ the yrast bands of these two isotopes can be associated with a similar deformed structure. In addition, these collective 8^+ levels move down in excitation energy with increasing N, from 5.3 MeV in ^{60}Fe$_{34}$ to 3.6 MeV in ^{64}Fe$_{38}$.

With this interpretation of the high-spin states in the neutron-rich Fe isotopes, an examination of the low-spin members of the yrast bands is in order. As N increases, the frequency at which the backbend takes place shifts to lower spin (Fig. 2). The cause underlying this feature is the compression in excitation energy of the entire level structure. In systems with shape coexistence, the explanation for such a compression is straightforward: as the deformed structures decrease in excitation energy, an interaction with the less deformed states occurs affecting both spherical and deformed level sequences.

Assuming this interpretation, two sets of states should be present in the Fe nuclei: a first corresponding to shell-model excitations with configurations involving neutrons in the fp shell, and a second associated with deformed states arising from the occupation of the $g_{9/2}$ neutron orbital. As already discussed above for ^{60}Fe, the excitation energies of the deformed states have been identified starting from the 8^+_1 state at 5333 keV. In Ref. [19], good agreement between shell-model calculations with the GXPF1A interaction and the data for the first 0^+, 2^+, 4^+, and 6^+ states suggest that these involve the coupling of $f_{7/2}$ protons and can, thus, be classified as "shell-model" states. If low-lying deformed levels are present as well, they must lie higher in excitation energy.

In Ref. [29], two excited 0^+ states were identified in ^{60}Fe following ^{60}Mn β decay. The excitation energies of these levels were also compared to shell-model calculations with the GXPF1 interaction. Good agreement between calculations and data was achieved for the 0^+_2 state with an energy difference of only 84 keV. In contrast, the 0^+_3 level at 2356 keV was found to lie 832 keV lower than the corresponding calculated value. As stated above, this deviation likely results from the fact that the configuration of this level cannot be described by considering particles in the fp space only, making it a good candidate for the 0^+ deformed excitation. Furthermore, a candidate for the 6^+ member of the deformed band has been identified in the fusion evaporation study of Ref. [19]. In the latter work, as many as five 6^+ levels were identified, even though the spin and parity assignments for two of these are tentative. The decay from the 8^+, $(g_{9/2})^2$ state is fragmented, and while the dominant decay branch proceeds toward a 7^- level, transitions to the 6^+_1, 6^+_2, and 6^+_5 states are observed as well. Based on energy systematics (E^5_γ factor), the decays to the 6^+_1 and 6^+_2 states should be favored over those to the 6^+_5

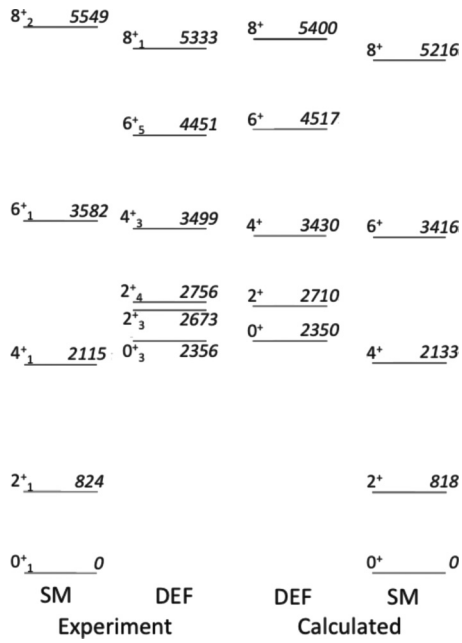

FIG. 3. Comparison between the experimental data and calculated shell-model (SM) and deformed (DEF) band structures in ^{60}Fe. The two experimental 2^+ levels shown are both candidates for a single deformed 2^+ state; see text for details. The SM levels were taken from Ref. [19] and, in the figure, are not mixed with the DEF states.

level by a factor of ∼30. The very fact that the deexcitation toward this 6^+_5 state is competitive indicates that its wave function must have a sizable overlap with that of the 8^+_1 level, making it a candidate for the 6^+ member of the deformed band. In order to find candidates for the 2^+ and 4^+ members of the deformed sequence, the data of Ref. [15] were revisited. This work reports on states observed in the β decay of the high-spin isomer ($I^\pi = 4^+$) in ^{60}Mn. Based on the location of the proposed 0^+ and 6^+ members of the deformed band, the 2^+_3 level at 2673 keV or the 2^+_4 one at 2756 keV and the 3499-keV 4^+_3 level are good candidates for the deformed sequence. In turn, the 8^+_2 level at 5549 keV of Ref. [19] can be viewed as a candidate for a shell-model state. Figure 3 presents the two families of levels separated according to the above comparisons.

Whether the selected states have indeed the spacing expected for a rotational band can then be ascertained through a comparison with the relations:

$$E_{4/2} = R, \quad \text{and} \quad E_{6/2} = R * 3.07 - 3.19, \qquad (1)$$

where $E_{4/2}$ and $E_{6/2}$ are the ratios of the excitation energies of the 4^+ and 6^+ states relative to the 2^+ level. This relationship between $E_{4/2}$ and $E_{6/2}$ was determined from the experimental data presented in Ref. [30] for values of R ranging from 3.0 and 3.33. While $R = 3.33$ corresponds to the $E_{4/2}$ value for a pure rotor, the correlation plot indicates that the relationship between $E_{4/2}$ and $E_{6/2}$ is continuous, correlated, and linear for $R = 3.0$ to 3.33 [30]. Using these expressions, values for the relative 2^+ energy of 360 keV and a value of R of 3.0, results in reasonable agreement with the experimental data with deviations of 69 and 67 keV for the 4^+ and 6^+ levels

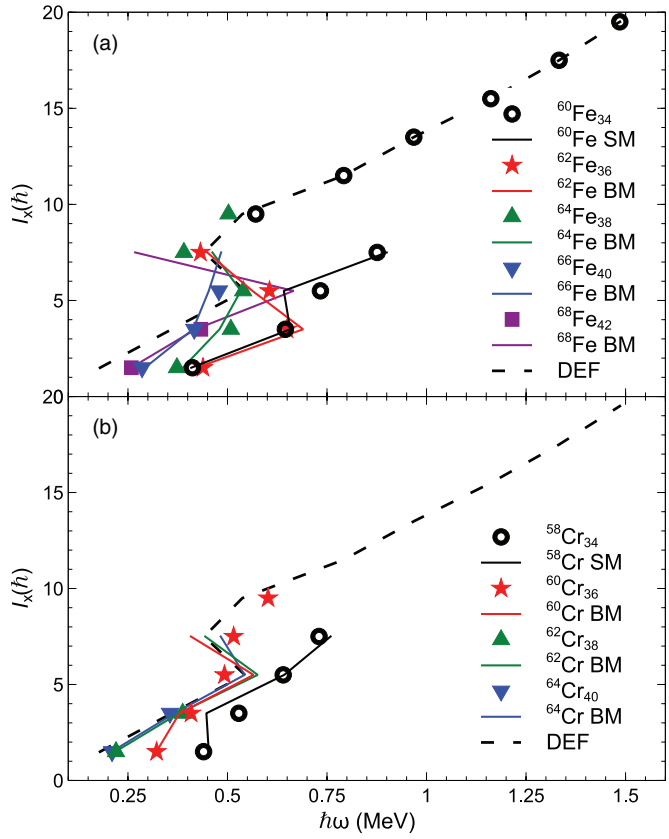

FIG. 4. (Color online) (a) I_x vs $\hbar\omega$ plots for the yrast bands in even Fe isotopes. Experimental data are given by symbols and the results of band-mixing calculations by solid lines for $^{62-66}$Fe (BM). For ^{60}Fe, the solid line is determined from the SM levels presented in Fig. 3. The dashed line represents the DEF trajectory determined from ^{60}Fe (see text for details). (b) Same plots for yrast bands in even Cr isotopes. BM results are presented for $^{60-64}$Cr and SM results for ^{58}Cr. The dashed line is the same as in panel (a).

as illustrated in Fig. 3. The goal here is not to reproduce precisely the levels proposed for the deformed band, but rather to use this parametrized sequence as a template for band-mixing calculations, as will become apparent below. In addition, Fig. 3 presents the shell-model calculations for ^{60}Fe using the GXPF1A interaction taken from Ref. [19] to illustrate that good agreement between experiment and calculations is obtained for the yrast shell-model states. Figure 4 presents the expected trajectory of the template rotational band as a dashed line in both Fig. 4(a) and 4(b). For $I = 8\ \hbar$ and higher, the experimental data associated with the $(g_{9/2})^2$ configuration in ^{60}Fe are used. For ^{62,64}Fe, the yrast bands are observed up to 8^+ and 10^+, respectively. In Fig. 4, both sequences begin on the shell-model trajectory represented by the low-spin states in ^{60}Fe, but end up on the deformed one in the I_x vs $\hbar\omega$ plane.

If these trajectories in Fig. 2 indeed result from shape coexistence between shell-model and deformed states, one should be able to reproduce the yrast bands using a simple state mixing model as presented in Eq. (2). Calculations of this type have been successfully employed in other regions of the nuclear chart where shape coexistence or band mixing influences the low-spin yrast line [22,31]. As discussed in

Ref. [22], the mixing between states with the same spin/parity can be described by the equation:

$$E_{\pm} = \frac{E_1 + E_2}{2} \pm \sqrt{\left\{\frac{E_2 - E_1}{2}\right\}^2 + V_{\rm int}^2}, \qquad (2)$$

where E_1 and E_2 are the energies of the unmixed levels and $V_{\rm int}$ is the interaction matrix element. Such calculations have been performed for ^{62}Fe and ^{64}Fe using the following parametrization. The unperturbed shell-model states were calculated using the GXPF1A interaction, and the relative energy spacing of the deformed 0^+, 2^+, 4^+, and 6^+ levels is taken as the template rotational band shown in Fig. 3. Every attempt was made to constrain the parameters as much as possible. Thus, $V_{\rm int}$ was set to 100 keV for all pairs of levels. This value seems reasonable based on the observations in ^{60}Fe. For example, the 8_1^+ (deformed) and 8_2^+ (spherical) states are separated by 206 keV. Assuming that the unmixed states lie at nearly the same energy, Eq. (2) would require $V_{\rm int}$ ~100 keV to reproduce the observed energy separation. A similar conclusion is reached with regards to the 2_3^+ and 2_4^+ states separated by 80 keV; i.e., $V_{\rm int}$ would be 40 keV maximally under the same assumption of nearly degenerate unmixed energies. One other condition is imposed on the deformed states: the 8^+ excitation energy is set to 3050 keV above the unmixed 0^+ state as was determined from ^{60}Fe after performing the band-mixing analysis. With these conditions, the single parameter to vary in the band-mixing calculations is the excitation energy of the deformed 0^+ state.

Figure 4 provides the results of these calculations in comparison with the experimental data in the I_x vs $\hbar\omega$ plane: reasonable agreement is achieved by setting the 0_2^+ energy to 1180 keV in ^{62}Fe and 680 keV in ^{64}Fe. In contrast to ^{60}Fe, where the deformed states become yrast starting at the 8^+ level, the deformed structures become yrast at the 4^+ level in ^{62,64}Fe. As stated above, the observed backbend behavior is a direct result of the crossing in energy of the two band structures and the resulting mixing.

Levels in ^{66,68}Fe are known only up to the $I^\pi = 6^+$ and 4^+, respectively [5]. The model is able to reproduce the observations by assuming $R = 3.33$ instead of the $R = 3.0$ value adopted for the lighter isotopes. In addition, the unperturbed 0^+ states of the rotational bands in the two isotopes must be further reduced in excitation energy to 200 and 125 keV, respectively, in order to approximate the observed energy levels. This results in the deformed states becoming yrast already at the $I^\pi = 2^+$ level with the first excited level in both isotopes being the deformed 0^+ state calculated to lie at an excitation energy of 240 and 180 keV, respectively. Due to the $N = 40$ gap, the shell-model calculations for the spherical states predict a spectrum which is drastically modified in ^{66}Fe relative to ^{64,68}Fe. Of particular significance is the lowering of the 6^+ state to 2300 keV in ^{66}Fe making it yrast in the present two-band mixing model. Thus, this simple model predicts that the 2^+, 4^+, and 8^+ yrast states in ^{66}Fe are of predominately deformed character, while the 0^+ and 6^+ states are dominated by wave functions with spherical components. This prediction could be readily tested by measuring lifetimes along the ^{66}Fe yrast sequence.

Turning the discussion to the Cr isotopes, rotational structures have been observed in ^{56,57}Cr, and in both isotopes at least one $g_{9/2}$ particle is included in the associated configuration [16,17]. Interestingly, ^{58}Cr stays on the shell-model trajectory in Fig. 4 suggesting that its 8^+ yrast state is associated with a spherical configuration in contrast with the observations in its isotone ^{60}Fe. This is likely due to the fact that the shell-model 8^+ level in ^{58}Cr lies nearly 1 MeV lower than the corresponding state in ^{60}Fe. This implies that the deformed 0^+ state in ^{58}Cr would have to lie at ~1.5 MeV in order to have the 8^+ level from the $(g_{9/2})^2$ configuration compete in excitation energy with the corresponding shell-model 8^+ state.

In contrast to ^{58}Cr, ^{60}Cr appears to exhibit a behavior attributable to band mixing with the 8^+ and 10^+ levels approaching the $(g_{9/2})^2$ trajectory defined by ^{60}Fe (Fig. 4). Zhu *et al*. were able to show that the GXPF1A Hamiltonian is unable to reproduce the observed ^{60}Cr level structure [17]. In the present band-mixing calculations, the excitation energy of the 2^+ state can be reproduced by assuming that the deformed band has a bandhead energy of 280 keV, a ratio $R = 3.1$, and all other parameters fixed as they were for the Fe isotopes. The resulting calculation has the deformed states becoming yrast already at the 2^+ level, and the predicted 8^+ state (whose excitation is kept constant at 3050 keV relative to the 0^+ level for all cases shown in Fig. 4) lies within ~100 keV of the observed 8^+ level at 3477 keV. The shell-model 8^+ level is in turn predicted to lie at 4.2 MeV. It is difficult to reproduce the excitation energy of both the 4^+ (1461 keV) and 6^+ (2466 keV) levels to better than 60 keV within the band-mixing model; however, the agreement is much better than that obtained with the GXPF1A Hamiltonian where these states are calculated to lie at 1819 and 2906 keV, respectively.

Only the first 2^+ and 4^+ states are known thus far in ^{62,64}Cr [4], and it is noteworthy that the 2^+ levels lie lowest in energy for these two cases. In fact, the trajectories of the low-spin states lie closest to the I_x vs ω trajectory represented by the phenomenological rotational band (Fig. 4); however, the $E_{4/2}$ ratio is only ~2.7. Performing the band-mixing calculation, the level energies can be reproduced by assuming a 2^+ to 0^+ energy difference of 360 keV and 350 keV for ^{62,64}Cr with $R = 3.1$ and $V_{\rm int} = 100$ keV. In both nuclei, the deformed 0^+ state is the ground state with the unmixed shell-model states placed at 5 and 50 keV, respectively. After mixing, the excited 0^+ states are at 200 and 206 keV and represent the first excited states in these nuclei. The two-band mixing calculations suggest a striking difference between the ground states of the ^{62,64}Cr nuclei and their isotones ^{64,66}Fe: while the latter are dominated by spherical configurations, the former appear to be associated with a deformed shape. It is possible that these conclusions provide an explanation for recent experimental observations. In Ref. [5], the inclusive two-proton knockout cross sections for ^{9}Be(^{68}Ni,^{66}Fe)X and ^{9}Be(^{66}Fe,^{64}Cr)X reactions were reported to differ by an order of magnitude with the latter measured to be only $\sigma_{\rm inc} = 0.13(5)$ mb. These observations suggest a lack of overlap between the ground-state wave functions in the latter case, consistent with the band-mixing calculations indicating a dominant spherical character for ^{66}Fe and a deformed one for ^{64}Cr. Similarly, inelastic scattering cross sections in ^{62,64,66}Fe and ^{60,62,64}Cr from ^{9}Be exhibit a

striking difference with N [4]: while the yields to the 2^+ levels are essentially constant in the Fe isotopes, a marked increase with N is seen in the Cr nuclei, consistent with ground- and yrast-state Cr configurations being dominated by deformed configurations near $N = 40$. It is worth noting that the large $B(E2)$ value measured for the 2^+ state in ^{66}Fe [8] is not inconsistent with the proposed interpretation as the 2^+_1 level is of dominant deformed character while the ground-state wave function exhibits significant admixture of spherical and deformed configurations.

A number of theoretical approaches have explored the structure of the Cr and Fe nuclei near $N = 40$; these include the spherical shell model [13,15], projected shell model [32], beyond mean field [11], and constrained Hartree-Fock Bogliubov + RPA [33] calculations. While differences exist in the configuration spaces under consideration and in the interactions used, these theoretical results are consistent with either shape coexistence or shape mixing and with ^{64}Cr exhibiting the largest degree of collectivity.

In summary, straightforward band-mixing calculations have been carried out in an attempt to reproduce the yrast bands of the neutron-rich ^{62,64,66,68}Fe and ^{60,62,64}Cr nuclei by invoking a shape coexistence picture inspired to a large extent by the extensive level structure available for ^{60}Fe. The approach constrained the model parameters as much as possible by keeping the interaction strength constant at 100 keV, by requiring the deformed 2^+ level to lie 360 keV above its 0^+ bandhead (except in ^{64}Cr where 350 keV was adopted), by limiting the R ratio to values between 3.0 and 3.3 and by requiring the $(g_{9/2})^2$ bandhead at 8^+ to lie 3050 keV above the deformed 0^+ state. A picture emerges of strongly mixed spherical and deformed configurations playing a major role at low spin near $N = 40$ in Cr and Fe, resulting in a dominant spherical ground state in ^{66}Fe and a deformed one in ^{64}Cr.

This work was supported by the US Department of Energy, Office of Nuclear Physics, under Contract No. DE-AC02-06CH11357.

[1] A. Gade *et al.*, Phys. Rev. C **74**, 021302(R) (2006).
[2] R. V. F. Janssens *et al.*, Phys. Lett. B **546**, 55 (2002).
[3] J. I. Prisciandaro *et al.*, Phys. Lett. B **510**, 17 (2001).
[4] A. Gade *et al.*, Phys. Rev. C **81**, 051304(R) (2010).
[5] P. Adrich *et al.*, Phys. Rev. C **77**, 054306 (2008).
[6] R. Broda *et al.*, Phys. Rev. C **86**, 064312 (2012).
[7] J. Ljungvall *et al.*, Phys. Rev. C **81**, 061301(R) (2010).
[8] W. Rother *et al.*, Phys. Rev. Lett. **106**, 022502 (2011).
[9] T. Baugher *et al.*, Phys. Rev. C **86**, 011305 (2012).
[10] N. Aoi *et al.*, Phys. Rev. Lett. **102**, 012502 (2009).
[11] J. N. Daugas *et al.*, Phys. Rev. C **83**, 054312 (2011).
[12] S. N Liddick *et al.*, Phys. Rev. C **84**, 061305(R) (2011).
[13] S. M. Lenzi, F. Nowacki, A. Poves, and K. Sieja, Phys. Rev. C **82**, 054301 (2010).
[14] K. Sieja and F. Nowacki, Phys. Rev. C **85**, 051301(R) (2012).
[15] N. Hoteling *et al.*, Phys. Rev. C **82**, 044305 (2010).
[16] A. Deacon *et al.*, Phys. Lett. B **622**, 151 (2005).
[17] S. Zhu *et al.*, Phys. Rev. C **74**, 064315 (2006).
[18] N. Hoteling *et al.*, Phys. Rev. C **74**, 064313 (2006).
[19] A. Deacon *et al.*, Phys. Rev. C **76**, 054303 (2007).
[20] D. Steppenbeck *et al.*, Phys. Rev. C **85**, 044316 (2012).
[21] M. Albers *et al.* (unpublished).
[22] M. P. Carpenter *et al.*, Phys. Rev. Lett. **78**, 3650 (1997).
[23] A. N. Andreyev *et al.*, Nature **405**, 430 (2000).
[24] F. G. Kondev *et al.*, Phys. Rev. C **62**, 044305 (2000).
[25] K. S. Bindra *et al.*, Phys. Rev. C **51**, 401 (1995).
[26] J. K. Deng *et al.*, Phys. Rev. C **52**, 595 (1995).
[27] W. C. Ma *et al.*, Phys. Rev. C **47**, R5 (1993).
[28] I. G. Bearden, Ph.D. thesis, Purdue University, 1993.
[29] S. Liddick *et al.*, Phys. Rev. C **73**, 044322 (2006).
[30] J.-P. Delaroche *et al.*, Phys. Rev C **81**, 014303 (2010).
[31] G. D. Dracoulis, Phys. Rev. C **49**, 3324 (1994), and references therein.
[32] Y. Yang, Y. Sun, K. Kaneko, and M. Hasegawa, Phys. Rev. C **82**, 031304(R) (2010).
[33] K. Sato *et al.*, Phys. Rev. C **86**, 024316 (2012).